FACULTY OF SCIENCE
PALACKÝ UNIVERSITY OLOMOUC

Department of Optics

Active phase stabilization of fiber interferometers for single photon measurements

DIPLOMA THESIS

Vojtěch Švarc

2018

FACULTY OF SCIENCE
PALACKÝ UNIVERSITY OLOMOUC

Department of Optics

Active phase stabilization of fiber interferometers for single photon measurements

DIPLOMA THESIS

Author:	Bc. Vojtěch Švarc
Study program:	B1701 Physics
Field of study:	Optics and Optoelectronics
Supervisor:	Mgr. Martina Nováková, Ph.D.
Co-Supervisor:	RNDr. Miroslav Ježek, Ph.D.

Date of submission: .....

PŘÍRODOVĚDECKÁ FAKULTA
UNIVERZITY PALACKÉHO V OLOMOUCI

Katedra optiky

Aktivní fázová stabilizace vláknových interferometerů pro měření na jednofotonové úrovni

DIPLOMOVÁ PRÁCE

Vypracoval:	Bc. Vojtěch Švarc
Studijní program:	B1701 Fyzika
Studijní obor:	Optika a optoelektronika
Vedoucí diplomové práce:	Mgr. Martina Nováková, Ph.D.
Konzultant diplomové práce:	RNDr. Miroslav Ježek, Ph.D.

Práce odevzdána dne: .....

Abstract

In this Thesis, active phase-lock of a fiber Mach-Zehnder interferometer is demonstrated. The phase-lock is performed with a strong signal that is perfectly separated from the single-photon measurement signal. Characterization of the phase-lock stability was performed using Fourier transform and Allan deviation. The slow phase drift, which is dominant, was decreased by 6 orders and the stabilization loop performs well up to 1 kHz. The setup behaves as a phase-tuned variable beam splitter. The possible splitting ratio is in the range from 0:100 to 100:0 with arbitrary step and with extinction more than 25 dB. The stability of various splitting ratios is measured and discussed. Further, the setup enables fast switching of an arbitrary splitting ratio employing an integrated electro-optic phase modulator. The fast switching was demonstrated for 5 ns pulses with rise time of 0.7 ns. The setup will be utilized for single-photon experiments with active feed-forward.

Keywords

Mach-Zehnder interferometer, active phase-lock, variable beam splitter, optical switch, polarization maintaining optical fibers.

Abstrakt

V rámci práce je realizován aktivně stabilizovaný vláknový Machův-Zehnderův interferometr určený k implementaci jednofotonových experimentů. Stabilizace fáze probíhá na silném optickém signálu, který je dokonale oddělen od měřicího jedofotonového signálu. V rámci práce byla odladěna stabilizační zpětnovazební smyčka a provedena její charakterizace pomocí Fourierovy transformace a Allanovy odchylky. Pomalý fázový drift, který je dominantní, byl utlumen o 6 řádů, přičemž celková šířka pásma stabilizační smyčky je 1 kHz. Stabilizovaný interferometr může fungovat jako dělič svazku s fázově laditelným proměnným dělicím poměrem. Variabilita nastavení dělicího poměru je od 0:100 do 100:0 s libovolným krokem a s extinkcí větší než 25 dB. Stabilita nastavených dělicích poměrů je měřena a diskutována v práci. Dále je umožněno rychlé spínání libovolného dělicího poměru pomocí implementovaného integrovaného elektro-optického fázového modulátoru. Rychlé spínání bylo demonstrováno pro 5 ns pulsy s dobou náběžné hrany 0,7 ns. Při budoucích jednofotonových experimentech bude rychlé spínání součástí dopředné vazby.

Klíčová slova

Machův-Zehnderův interferometr, aktivní fázová stabilizace, dělič svazku, proměnný dělicí poměr, optický přepínač, polarizaci udržující optická vlákna.

Acknowledgement

First of all, I would like to express my sincere gratitude to my supervisor Mgr. Martina Nováková, Ph.D. and to my co-supervisor RNDr. Miroslav Ježek, Ph.D. for guidance, patience, and advices. My thanks also go to my lab colleagues Josef Hloušek, Radim Hošák, Jaromír Mika, Robert Stárek, Ivo Straka, and others for friendly environment, kindness, and useful hints. Last but not the least, I would like to thank my family for their care and continuous support.

Declaration

I declare that I have written the Thesis "Active phase stabilization of fiber interferometers for single photon measurements" on my own under the guidance of Mgr. Martina Nováková, Ph.D. and RNDr. Miroslav Ježek, Ph.D. by using theoretical resources, which are referred to in the list of literature. I agree with the further usage of the Thesis according to requirements of Palacký University Olomouc.

In Olomouc .....

Contents

1 Introduction

Interference is the most important consequence of wave character of the light. Light split into two parts and again combined together interferes – not intensities of the two light signals, but their amplitudes are superposed, thus the resulting intensity distribution is dependent on relative phase between the two signals. Measurement devices based on this effect are called interferometers. Some of the most famous configurations are Michelson and Mach-Zehnder interferometers [1]. They have wide range of application, including precise measurement of surfaces [2], holography [3], and high-resolution imaging [4]. Interferometers are also implemented in various quantum optics experiments. For instance, they are utilized in schemes for teleportation [5], entanglement swapping [6], and loophole-free violation of Bell inequalities experiments [7, 8]. All of these quantum optics experiments aim for possible application in inherently secure communication, utilizing quantum properties of the light. Furthermore, it was shown that linear optics scheme based on Mach-Zehnder interferometers is suitable for quantum computing [9].

The universal property of the quantum system is an inherent randomness. One of the consequence is that quantum state projection performed by a measurement is just probabilistic, not deterministic. Hence quantum optics schemes are mostly probabilistic and with increasing dimension of Hilbert space, the probability of success of an exact operation rapidly decreases. Fortunately, the probability of success can be improved by using a technique of feed-forward. It means that the result of measurement of a photon will be used to trigger some operation on another propagating photon. For example, the feed-forward technique was used to enhance the success of probability of quantum gate based on linear optics [10].

Another consequence of the probabilistic character of quantum mechanics is that conventional sources of single-photons cannot generate photons on demand, but the photons are generated randomly and there is some probability of generating more than one photon. There are some genuine single-photon sources as quantum dots, but their total efficiency is still low [11]. Fortunately, the performance of the conventional single-photon sources based on spontaneous parametric-down conversion can be improved with feed-forward using a fast optical switch which would enable to conditionally switch optical signal between two ports. Photons that are randomly generated in pairs via spontaneous parametric-down conversion are multiplexed in time or space and released on demand [12, 13, 14]. Another approach is utilization of an optical shutter, which is a switch with just one output port that is either open or closed. Opening the shutter for a short period of time when a photon is heralded enables to produce light with sub-Poissonian statistics [15, 16].

Furthermore, the optical switch can be utilized in many linear-optical circuits. Fast optical switch is an important element of various time-bin encoding schemes, where the signal has to be variable switched between several delay loops. For example, recent universal quantum computing scheme requires fast switch with high tunability [17]. Feed-forward featuring a fast optical switch was also recently utilized to obtain genuine time-bin entanglement [8].

Many experiments mentioned before are restricted by speed of the switching, thus there is a huge effort to realize an ultra-fast optical switch. The simplest idea how to implement

an optical switch, is utilization of a polarization beam splitter and a polarization switch. A recent experiment utilizes Pockels cells with tuning performance close to 10 ns and repetition rate of 500 kHz [14]. However, a required voltage in the order of kilovolts is still limiting for polarization-based ultra-fast switching. Nevertheless, ultra-fast switching can be provided with an electro-optic phase modulator placed in one arm of a Mach-Zehnder interferometer. For this purposes a fiber implemented Mach-Zehnder interferometer is more convenient because integrated electro-optic phase modulators have much faster response then the free-space ones. Using the fiber interferometer, the signal can be theoretically switched even on sub-nanosecond scale.

Unfortunately, interferometers are affected by spontaneous phase changes caused by ambient temperature instability, air flux, and vibrations. To provide correct performance of the interferometric switch, phase has to be actively stabilized. Nevertheless, proper stabilization of single-photon setups is complicated [7, 18, 19, 20]. Due to statistical character of light, photon count rates vary, thus phase is estimated with an error. Despite of this fact, continuous phase-lock at single-photon level is possible but its speed is typically no more than 10 Hz [18]. In addition, when single-photon signal is used for the actual measurement, it cannot be simultaneously used for the stabilization. Then the stabilization process and the measurement have to be periodically switched [10]. However, this step-by-step stabilization procedure increases data acquisition time and the phase is not under control continuously. To evade this problems, another signal used only for the stabilization purposes can be added to the interferometer. The point is that the stabilization signal can be much stronger than the single-photon one, thus the phase can be evaluated continuously and with low error. It means that the continuous phase-lock with fast response is provided. However, to avoid unwanted crosstalk from the stabilization signal to the single-photon measurement signal, excellent separation of the signals is required.

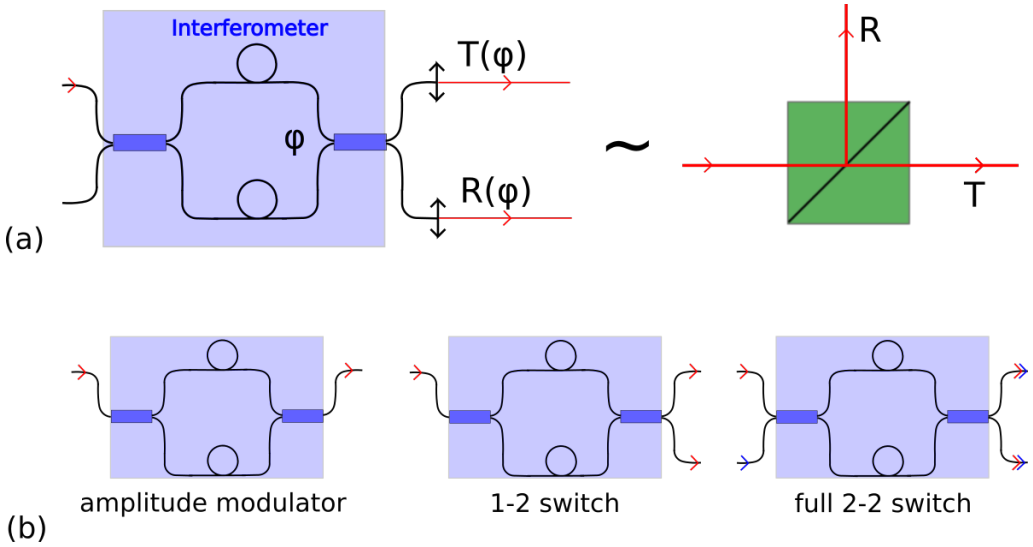

Figure 1: (a) Interpretation of a Mach-Zehnder interferometer as a beam splitter. (b) Possible configuration of the interferometric beam splitter in dependence on number of used ports.

The Aim of this Thesis is to implement a continuous phase-lock in fiber Mach-Zehnder interferometer used for single-photon measurements. The phase-lock is performed with strong continuously detected signal that has a different wavelength than the single-photon measurement signal. The setup allows for an arbitrary phase difference between the signals and, moreover, fast switching of arbitrary phase on the sub-nanosecond scale is enabled by the integrated electro-optic phase modulator. Since in the architecture of Mach-Zehnder interferometer both output ports are available, this setup can be utilized as a variable beam splitter, where the splitting ratio is tuned as a phase in the interferometer as shown in Fig. 1 (a). The interferometric beam splitter can perform in more configurations depending on utilized interferometer ports. It is depicted in Fig. 1 (b). Firstly, it can be used as an optical shutter (amplitude modulator) if just one input and one output ports are used. Secondly, it can perform as a 1-2 optical switch if one input and two output ports are utilized. Thirdly, it can serve as a combiner of two optical signals (2-2 switch) if all the interferometer ports are utilized. In this Thesis, only the configuration of the 1-2 switch is used. In future, the setup will be utilized for single-photon experiments using active feed-forward. For instance, experiments enabling conditional modification of statistic of light are planned. Further, the setup will be utilized for quantum thermodynamics simulations, where the configuration of the 2-2 switch will be utilized.

The further text is structured to three main chapters. The chapter 2 is about tools and methods relevant to the experiment. In the chapter 3, an experimental setup consisting of optical and electronic parts is described. In the chapter 4, we present results of setup stability, splitting ratio tunability, and fast switching.

2 Methods and tools

Let us introduce a basic scheme of the experiment shown in Fig. 2. As mentioned before, the scheme consists of fiber Mach-Zehnder interferometer, where an integrated electro-optic phase modulator (EOM) enabling the fast phase switching is placed in one arm. Measurements are performed with measurement signal (yellow dots). To avoid unwanted random phase fluctuation in the interferometer, it is stabilized with active phase stabilization feedback loop including a detector, a PID controller, and a phase modulator. For stabilization purposes, an extra signal called stabilization signal (red line) is implemented. Stabilization signal propagates through the same path as the measurement signal, thus it is affected by the same phase fluctuations. Due to a necessity of spatial separation of both signals at the outputs, they have different wavelengths (the separation part is not explicitly shown).

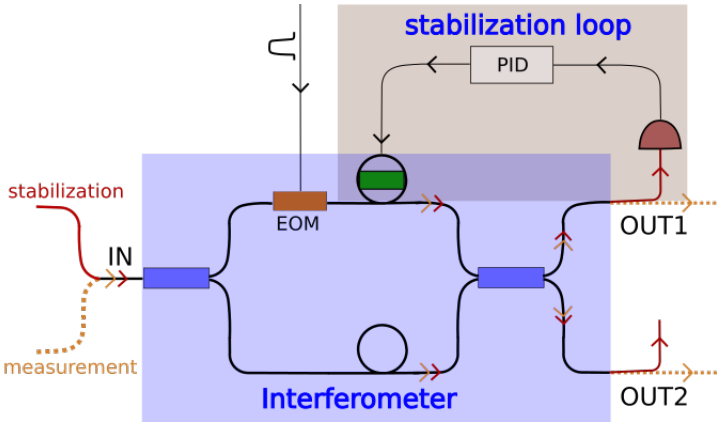

Figure 2: Basic scheme of the experiment. Fiber Mach-Zehnder interferometer is phase-locked with the stabilization loop. An integrated electro-optic phase modulator (EOM) is implemented in one interferometer arm to provide fast switching.

In this chapter, we introduce some tools and methods important for the experiment. In sections 2.1 and 2.2, Mach-Zehnder interferometer and phase evaluation are described. In section 2.3 problems of having two different wavelengths in the interferometer are discussed. In section 2.4 a device for manipulating a phase difference between the wavelengths is described. It is followed by a description of the wavelengths separation in section 2.5. Action of the stabilization loop is discussed in section 2.6. Allan variance, which is a tool for analyzing a stability of the interferometer, is introduced in section 2.7.

2.1 Mach-Zehnder interferometer (MZI)

Mach-Zehnder interferometer (MZI) is an optical device with two inputs and two outputs [1]. Fiber implementation of the interferometer is shown in Fig. 3(a). Incident beam is divided by fiber coupler FC1 into two arms with length L_1 and L_2. The two parts of the beam again meet on fiber coupler FC2 and interfere, assuming that the coherence length of the beam is high enough. Output intensities I_{out1} and I_{out2} depend on phase φ in the interferometer. The

phase is proportional to a path difference of the arms $\Delta L = L_1 - L_2$. An ideal interference pattern is shown in Fig. 3(b). The pattern is harmonic function and it is called interference fringe. Total intensity $I_{\text{total}} = I_{\text{out1}} + I_{\text{out2}}$ is independent of phase which is a consequence of law of conservation of energy. In reality, interference fringes do not reach the zero intensity. For characterization of the quality of interference, the visibility parameter V is defined,

$$V = \frac{I_{\max} - I_{\min}}{I_{\max} + I_{\min}}, \tag{1}$$

where $I_{\max}$ is maximum intensity and $I_{\min}$ is a minimum intensity of the interference fringe. The higher number of visibility, the better interference. Generally, visibilities for output ports OUT1 and OUT2 are different.

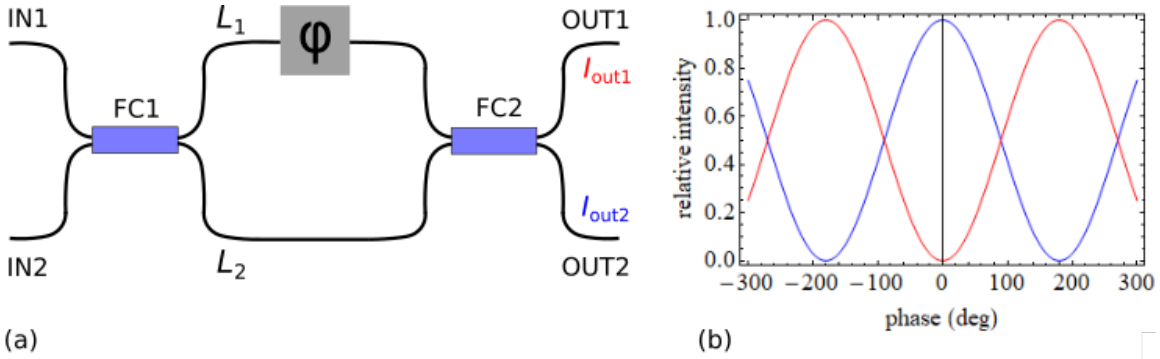

Figure 3: (a) Scheme of fiber Mach-Zehnder interferometer. Input beam is divided on fiber coupler FC1 into two independent arms. Two parts of the beam again meet on fiber coupler FC2 and they interfere. The interference is observed like phase-dependent intensity on output ports (OUT1, OUT2). (b) Interference fringes, output intensity of ports I_{out1} (red) and I_{out2} (blue) in dependence of phase.

Generally, visibility depends on various parameters such as temporal, spectral, spatial and polarization mode overlap of the interfering light. In single-mode fiber implementation of the MZI, spatial overlap (overlap of transverse modes) is guaranteed. Also, it is convenient to utilize polarization-maintaining fibers to secure polarization overlap. Spectral overlap is maximized provided that dispersion in the two arms is the same.

Further, to reach excellent visibility in MZI, it is important to balance amplitudes of the interfering light. The amplitudes are dependent of loss in the arms and properties of FC1, FC2 such as splitting ratio and insertion loss. If the loss in each arm can be tuned and only one input port of FC1 is utilized, then the most important parameter for visibility is just splitting ratio of FC2. The highest visibility for both output ports can be achieved with balanced FC2 (50:50). However, even for unbalanced one, it is still possible to have maximal visibility for at least one output port. For more complex analysis see references [21, 22].

As mentioned in the introduction, MZI can be interpreted as a variable beam splitter with splitting ratio $T : R$ depending on the phase in MZI. To keep relation $T + R = 1$, transmittance T and reflectance R are set as

$$T = \frac{I_{\text{out1}}}{I_{\text{out1}} + I_{\text{out2}}}, \tag{2}$$

and

$$R = \frac{I_{\text{out2}}}{I_{\text{out1}} + I_{\text{out2}}}. \tag{3}$$

Note that T and R are interchangeable. It means that we can choose, which output represents the transmitted port and which one represents the reflected port.

2.2 Phase-evaluation of MZI

To characterize phase fluctuation of an interferometer, an evaluation from intensity to phase has to be developed. Firstly let us assume that visibility V of the output ports OUT1 and OUT2 is the same. If there are not any losses on OUT1 and OUT2, the output intensities are

$$\begin{aligned} I_{\text{out1}} &= I_0(1 + V\cos\varphi), \\ I_{\text{out2}} &= I_0(1 - V\cos\varphi), \end{aligned} \tag{4}$$

where I_0 is half of the total intensity and φ is the phase of the interferometer. The total intensity is $I_{\text{out1}} + I_{\text{out2}} = 2I_0$, thus the I_0 can be replaced. Finally, the expression for the phase is given as

$$\varphi = \arccos\left[\frac{1}{V}\left(\frac{2I_{\text{out1}}}{I_{\text{out1}} + I_{\text{out2}}} - 1\right)\right]. \tag{5}$$

Note that the evaluated phase φ is not the absolute phase, though the relative one. When the phase changes of 2π, the output intensity becomes the same. However, measurement of the absolute phase is not our object of interest

Now we will describe the more complicated, but realistic model. Firstly, the visibilities of the outputs OUT1 and OUT2 are different. Thus we replace the visibility V from eq. (4) to V_1 and V_2. Secondly, the detected signal includes some offset from the detectors. Generally, each detector has different offset off_1 and off_2. Thirdly, there are some losses on the output ports of the interferometer and it is different for OUT1 and OUT2. Also, efficiencies of the detectors differ. Hence the coefficients I_0 from eq. (4) should be replaced with some I_{01} and I_{02}. In general, detected output intensities I_{D1}, I_{D2} are

$$\begin{aligned} I_{\text{D1}} &= I_{01}(1 + V_1\cos\varphi) + \text{off}_1, \\ I_{\text{D2}} &= I_{02}(1 - V_2\cos\varphi) + \text{off}_2. \end{aligned} \tag{6}$$

Note that sum $I_{\text{D1}} + I_{\text{D2}}$ is phase-dependent, thus it is not equal to total intensity. Now assume that some electronic or software processing of detected signal is available. It enables to simplify eq. (6) and receive equation similar to eq. (4). Firstly, we subtract the offsets off_1 and off_2. Secondly, we balance the output ports to keep phase-independent total intensity. Due to the balancing procedure coefficient $I_{02} \to I_{01}\frac{V1}{V2}$. The resulting intensities are[1]

[1]Note that I_{out1} and I_{out2} from eq. (4) is different from I_{out1} and I_{out2} from eq. (7). It is due to difference between the simplified model and the realistic one.

$$I_{\text{out1}} = I_{01}(1 + V_1 \cos\varphi), \tag{7}$$
$$I_{\text{out2}} = I_{01}\frac{V_1}{V_2}(1 - V_2 \cos\varphi).$$

From eq. (7) the equation for phase similar to eq. (5) is derived as

$$\varphi = \arccos\left[\frac{1}{V_1}\left(\frac{I_{\text{out1}}\left(1+\frac{V_1}{V_2}\right)}{I_{\text{out1}} + I_{\text{out2}}} - 1\right)\right]. \tag{8}$$

Note that if $V_1 = V_2$ than eq. (5) is identical to eq. (8). The equation (8) is used for phase-evaluation in our experiment. Unfortunately, there are still few problems, especially for longer measurements. Parameters V_1, V_2, I_{01}, and I_{02} slightly changes in time as a consequence of the setup detuning. Therefore with increasing time of measurement the eq. (8) begin slightly inaccurate. However, for measurement durations in the order of tens minutes it is usually negligible. The algorithm for evaluating phase from the measured intensity is described in Appendix A.

2.3 MZI with two wavelengths

In this section, MZI operating with two beams with different wavelength λ_1 and λ_2 will be discussed. For simplicity let us assume that dispersion is negligible and MZI has only one input and one output as shown in Fig.4(a). The phase φ now depends not only on length difference ΔL, it also depends on wavelength. The interference fringes have a different period for the λ_1 and λ_2, see Fig. 4(b).

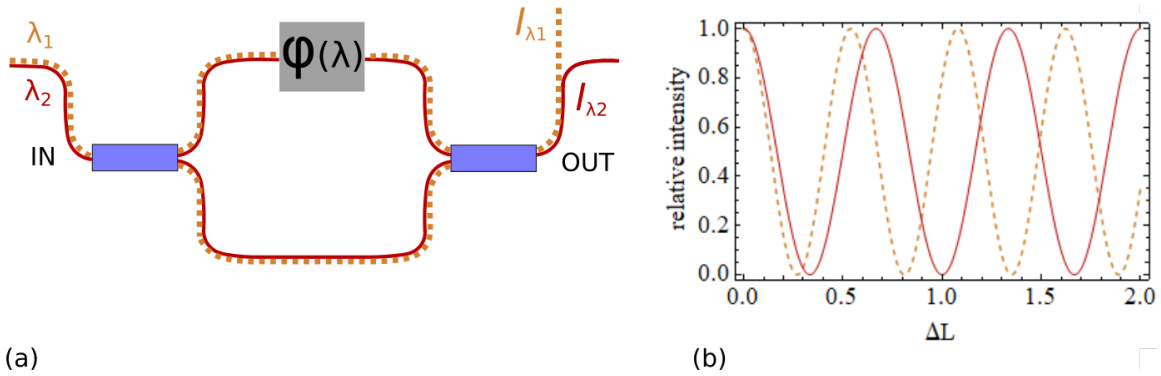

Figure 4: (a) Scheme of fiber MZI with two different wavelengths λ_1 (yellow dots) and λ_2 (red line). (b) Interference fringes of two different wavelengths in an ideal MZI.

Important parameter is the phase difference $\Delta\varphi$ between the beams:

$$\Delta\varphi = \varphi(\lambda_1) - \varphi(\lambda_2) = 2\pi n \Delta L\left(\frac{1}{\lambda_1} - \frac{1}{\lambda_2}\right), \tag{9}$$

where n is refractive index of optical fiber.

For typical parameters of our interferometer $\lambda_1 = 810$ nm, $\lambda_2 = 830$ nm, $\Delta L = 5$ μm and $n \cong 1.5$ the phase difference is $\Delta\varphi \cong 0.5\pi = 90°$. It is obvious that only if $\Delta L = 0$, the phase difference $\Delta\varphi = 0$. However, it would be convenient to tune arbitrary phase difference $\Delta\varphi$ and also to be in the maximum of the autocorrelation function ($\Delta L \approx 0$). It is possible with phase dispersive element described in next section.

2.4 Phase dispersive element

In this section and further, dispersion has to be taken into account, thus refractive index $n = n(\lambda)$. Phase dispersive element is a device for setting phase difference $\Delta\varphi$ between two beams with different central wavelengths λ_1 and λ_2. It consists of two plane-parallel plates from a high-dispersion glass as shown in Fig. 5. If one plate is slightly rotated, optical path increases. The point is that due to the dispersion the optical path for λ_1 and λ_2 is different, thus the $\Delta\varphi$ changes. Therefore $\Delta\varphi$ is also function of angle of rotation α. Symmetric rotation of the second plate compensates beam displacement Δy.

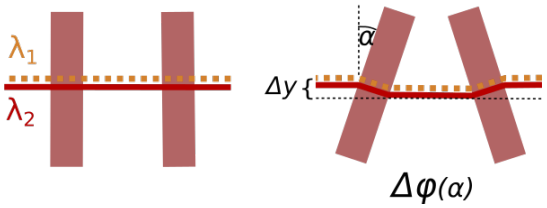

Figure 5: Phase dispersive element for manipulating phase difference $\Delta\varphi$ between λ_1 and λ_2 in MZI. It consists of two plane-parallel plates from dispersive material. With the increasing angle of rotation α the optical path increases. The longer optical path in dispersive material, the higher dispersion between λ_1 and λ_2 is. Second plate is used for elimination of the beam displacement Δy.

Now the phase dispersive element will be discussed in more detail. The situation for a single wavelength is depicted in Fig. 6. The beam entering the plane-parallel plate with an angle of incidence α_1 is refracted with the angle α_2. From Snell's law [23]

$$\alpha_2 = \arcsin\left(\frac{n_0}{n}\sin\alpha_1\right), \tag{10}$$

where n_0 is refractive index of air and n is refractive index for the dispersive material of the plate. Now we are interested in the path x of the beam in the plate:

$$x = \frac{d}{\cos\alpha_2}, \tag{11}$$

where d is thickness of the plate. Crucial for changing $\Delta\varphi$ is ability to change $\Delta x = x - d$. From (10) and (11) the equation for Δx is derived:

$$\Delta x = x - d = \frac{d}{\cos\left[\arcsin\left(\frac{n_0}{n}\sin\alpha_1\right)\right]} - d. \tag{12}$$

This is quite complicated, however, for small angle of incidence $\sin\alpha_1 \approx \alpha_1$. Then (12) has simplified form

$$\Delta x \approx \; d\left[\frac{1}{\cos\left(\frac{n_0}{n}\alpha_1\right)} - 1\right]. \tag{13}$$

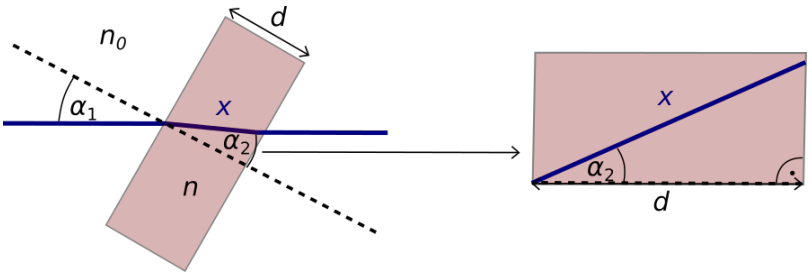

Figure 6: Mathematical description of beam passing through plane-parallel plate. On the right there is a detail view of the plate.

Important parameter for characterization of the phase dispersive element is relative phase difference $\Delta\varphi_r$ given as

$$\Delta\varphi_r = 2\pi\left(\frac{o_1}{\lambda_1} - \frac{o_2}{\lambda_2}\right), \tag{14}$$

where o_1 and o_2, respectively, denote optical path in dispersive material for λ_1 and λ_2, respectively. Thus $\Delta\varphi_r$ is the phase difference between λ_1 and λ_2 caused just by the effect of dispersion. In other words, it can be interpreted as a displacement of maxims of autocorrelation functions for two different wavelengths.

Now assume that λ_1 and λ_2 are close to each other. Then the dispersion is small and angle of refraction $\alpha_2(\lambda_1) \approx \alpha_2(\lambda_2)$. Thus geometrical paths for both wavelengths are $\Delta x(\lambda_1) \approx \Delta x(\lambda_2)$. Then from (13) and (14) the equation for $\Delta\varphi_r$ caused by the phase dispersive element is given as

$$\Delta\varphi_r = 2\pi\Delta x\left[\frac{n(\lambda_1)}{\lambda_1} - \frac{n(\lambda_2)}{\lambda_2}\right] \approx 2\pi d\left[\frac{1}{\cos\left(\frac{n_0}{n}\alpha_1\right)} - 1\right]\left[\frac{(n(\lambda_1)}{\lambda_1} - \frac{n(\lambda_2)}{\lambda_2}\right], \tag{15}$$

where n is an average value of refractive index for λ_1 and λ_2. Equation (15) for typical parameters is shown in Fig. 7 (a). Fig. 7 (b) shows an error caused by the approximation $\alpha_2(\lambda_1) \approx \alpha_2(\lambda_2)$. The relative error is less than 1% even for $\alpha = 30°$.

Phase dispersive element should have an ability to tune $\Delta\varphi_r$ from 0 to π or more. On the other hand, the angle of incidence α_1 cannot be arbitrary. According to Fresnel equations, with increasing α_1 the transmittance decreases and the interferometer is detuned. This could be partially compensated with anti-reflection coatings of the plate. Also, with increasing α_1 the diameter of the plate has to increase. Thus the range of angle of incidence is a restriction. Also, there is different transmittance for TE and TM polarization, thus it is necessary to avoid random fluctuation of polarization in the setup. In our setup, polarization is kept constant due to polarization maintaining fiber implementation of the interferometer.

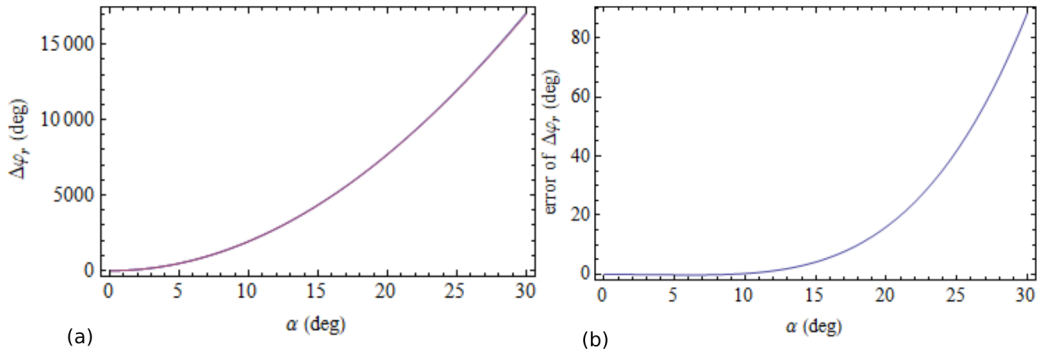

Figure 7: (a) Equation (15) for typical parameters $\lambda_1 = 810$ nm, $\lambda_2 = 830$ nm, and for glass plate from SF10 with thickness d=2 cm. Refractive indexes of SF10 are from [24]. (b) Error caused by the approximation $\alpha_1(\lambda_1) \approx \alpha_1(\lambda_2)$.

Photo of a prototype of the phase dispersive element is shown in Fig. 8(a). The plates are mounted in home-made manual rotation stage consisting of metallic toothed wheels and 3D printed components[2] from polylactide (PLA). An advantage of this stage comparing to commercial rotation stages is that both plates rotate simultaneously. This is achieved with the two toothed wheels working together. Thus the beam displacement Δy is automatically eliminated.

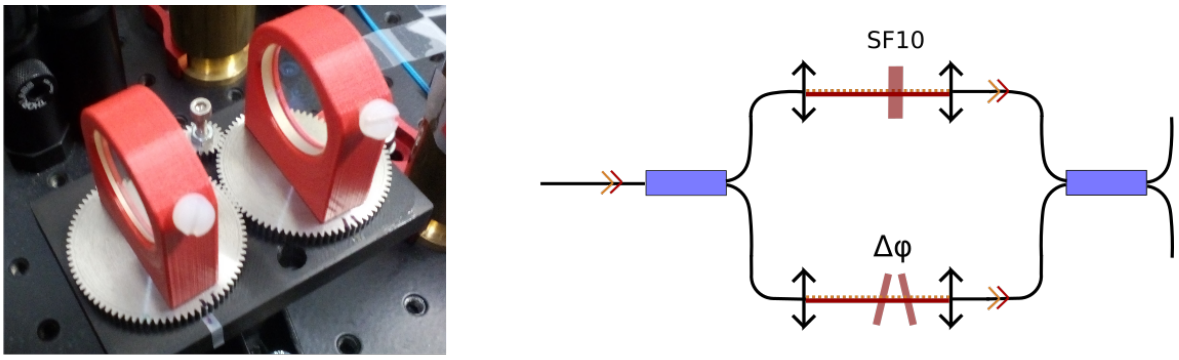

Figure 8: (a) Prototype of phase dispersive element that we developed for our experiment. The plates rotate simultaneously due to the gear. (b) Implementation of phase dispersive element into Mach-Zehnder interferometer. The plate from SF10 glass in the upper arm compensates dispersion "offset" caused by the phase dispersive element $\Delta\varphi$ placed in the lower arm.

The plane-parallel plates from SF10 glass with thickness $d = 10$ mm and diameter 25 mm are used. It has an anti-reflective coating for angles of incidence in range of 0-30°and wavelengths in a range of 780-850 nm. The relative phase difference of the device is more than $\Delta\varphi_r > \pi$ for the angle of incidence $\alpha_1 < 5°$. Intrinsic loss of the device is negligible for angles of incidences up to 30°. The only problem is that the dispersion in one arm of the interferometer rapidly increases.

[2]The mechanical parts of the stage were designed by Martina Nováková. It was processed and 3D printed by Petr Novák.

This is solved by adding the same glass with thickness 20 mm to the second arm, as shown in Fig. 8(b).

2.5 Separation of two different wavelengths

We have already mentioned Mach-Zehnder interferometer operating with two beams with different central wavelengths. Now the question is how to separate the wavelengths at the output of the interferometer. There are several possibilities how to do that. For example, the use of diffraction grating is possible. However, there is a significant loss of the optical power due to diffraction to higher orders. Especially in single-photon experiments, the losses are undesirable.

We perform the wavelength separation with an optical isolator shown in Fig. 9. It consists of a polarizing beam splitter (PBS), a quarter-wave plate (QWP) and an interference filter (IF) with high extinction ratio. The angle between optical axis of the QWP and horizontal polarization is 45°.

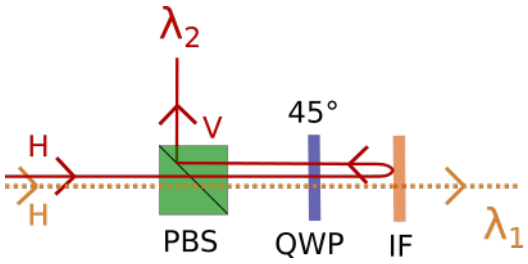

Figure 9: Scheme of the optical isolator. Its purpose is to separate beams with different wavelength λ_1 and λ_2. H – horizontal polarization, V – vertical polarization, PBS – polarization beam splitter, QWP – quarter-wave plate, IF – interference filter

.

Incident beams with central wavelength λ_1 and λ_2 are both horizontally polarized. Thus they both pass through the PBS. Subsequently, they pass through the QWP, so the polarization changes from horizontal to right-handed circular. Then IF transmits the beam with λ_1 and reflects the beam with λ_2. For the reflected beam the polarization changes to left-handed circular. The beam again passes through QWP, so the polarization switches to vertical which is reflected on PBS. Thus the beams are spatially separated from each other.

2.6 Active phase stabilization feedback loop

To avoid the random phase fluctuation of the MZI, it is necessary to stabilize the setup. In some cases, it is sufficient to use just passive stabilization. It means that the setup stands on anti-vibration optical table and it is covered to eliminate the air flux. However, especially for long-time stability and fiber experimental setups, it is not sufficient. Then the passive stabilization has to be supported by active stabilization which compensates the phase fluctuations in real-time.

A scheme of our active phase stabilization feedback loop is shown in Fig. 10. It consists of detector(s), PID controller [25], and piezoelectric fiber stretcher [26] which is placed in one arm

of the interferometer. Fiber stretcher is a phase modulator with high dynamic range. It works on the principle of stretching the fiber wounded around a piezoelectric crystal.

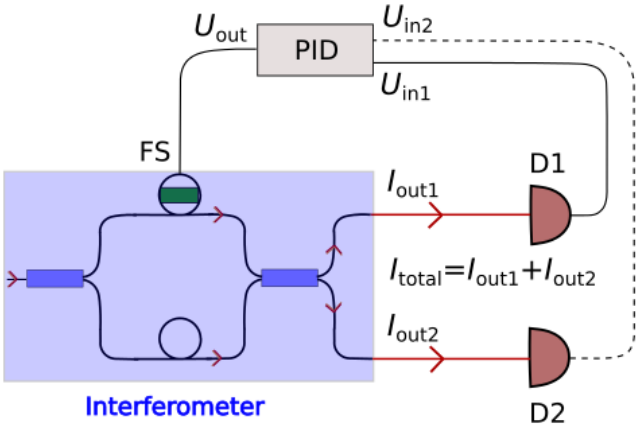

Figure 10: Scheme of the active phase stabilization feedback loop of MZI. Phase fluctuation causes change of I_{out1}. Detector (D1) converts I_{out1} into U_{in1} and it is evaluated in the PID controller. Output voltage U_{out} is applied to fiber stretcher (FS). It compensates the phase fluctuations by increasing or decreasing the length of one arm of the interferometer. If also detector D2 is used, the feedback loop keeps the desired phase regardless to total intensity change.

The basic principle of the feedback loop is: Phase fluctuations, which correspond to intensity detected, are evaluated in PID controller. Than PID controller simply puts corresponding voltage U_{out} to fiber stretcher, so the optical path is increased or decreased and the phase is kept constant.

In more detail, phase fluctuations inside interferometer are observed as optical intensity fluctuations of I_{out1} and I_{out2} according to interference law. Intensities I_{out1} and I_{out2} are detected by detectors D1 and D2, respectively, and a corresponding voltage U_{in1} and U_{in2} is generated. The phase fluctuations are evaluated from an error signal U_{err}, which is difference between U_{in1} and a reference signal U_{set}. In regime when just one output of MZI is available (D1 is used only), U_{set} is generated from an external source as a constant voltage. Then stabilized I_{out1} corresponds to desired phase only if total intensity $I_{\mathrm{total}} = I_{\mathrm{out1}} + I_{\mathrm{out2}}$ is constant. However, when both outputs of MZI are available, D2 is used as well and U_{set} is derived from total intensity I_{total}. While I_{total} changes, U_{set} changes proportionally. Thus the correct phase is stabilized regardless of fluctuations of I_{total}.

So far we pretended that stabilization loop performance is ideal. However, like all other electronic devices, it is limited by its bandwidth and dynamic range. Now the situation when stabilization fails will be described. If a phase changes so fast and with high amplitude, the phase changes from φ to $\varphi + m\pi, m = 1, 2, ...$, where it is locked again. Thus the relative phase does not change but the absolute one changes. To reduce this effect phase-lock in the middle of interference fringe should be used ($\varphi = \frac{\pi}{2} + m\pi$). In addition, it is place with the highest derivation $\frac{dI_{\mathrm{out1}}}{d\varphi}$, thus random phase fluctuation causes the highest change of U_{in1}. Therefore the best performance of the stabilization is in the middle of the interference fringe.

In the experiment, we utilized both interferometer outputs and we operated with stabilization signal roughly in the middle of the interference fringe.

2.7 Allan variance

Allan variance is a useful tool for quantifying the phase error in long-time stability measurement. Basically, it is a variation depending on duration τ of measurement. For particular τ the error of the measurement is the lowest possible. Therefore it helps us to set optimal time interval of measurement and investigate the stability [27, 28].

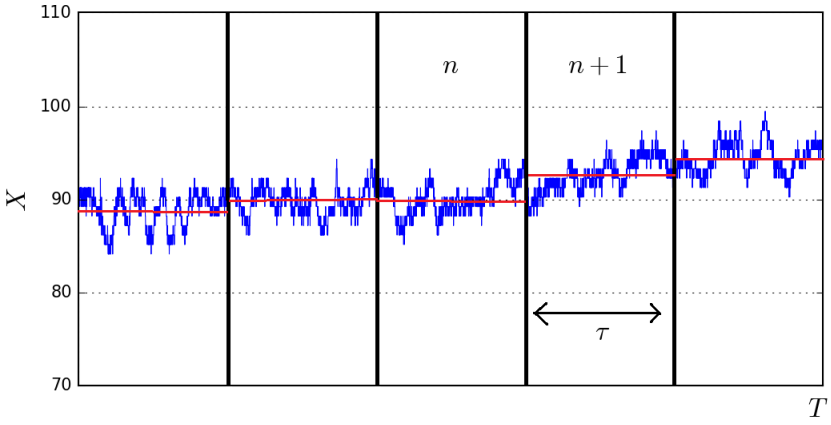

Figure 11: Principle of Allan variation.

The principle of this method is described in Fig. 11. Data from a measurement accumulated for overall time T are divided into N subsets with identical duration τ. Mean value of each subset is evaluated and the mean value of the subset n is subtracted from the mean value of the subset $n+1$. These particular results are squared, summed and normalized. Allan variance is given as

$$\mathrm{Var_A}\left(\tau\right) = \frac{1}{2N}\sum_{n=1}^{N-1}\left(\langle X\rangle_{n+1} - \langle X\rangle_n\right)^2, \tag{16}$$

where $\langle X\rangle_n$ is the mean value of the n-th subset.

Analogically to classical deviation, the Allan deviation σ_A is defined as square root of $\mathrm{Var_A}$,

$$\sigma_\mathrm{A}\left(\tau\right) = \sqrt{\mathrm{Var_A}\left(\tau\right)}. \tag{17}$$

For characterization of a measurement, Allan deviation is usually used instead of Allan variance, since it has the same dimension as the measured quantity.

3 Experimental setup

The experimental setup is shown in Fig. 12 and its photo is shown in Appendix C. It is actively stabilized fiber MZI operating with two optical signals with different central wavelengths. The first one is used for stabilization and the second one is used for measurement purposes. The stabilization signal usually has 2-4 orders of magnitude higher optical power. During single-photon measurements, it has the optical power of about 100 pW. The setup consists of several parts: Preparation of the optical signals, the interferometer, separation part and electronic part. Some of them are described in more details further, however, firstly the whole setup is briefly described.

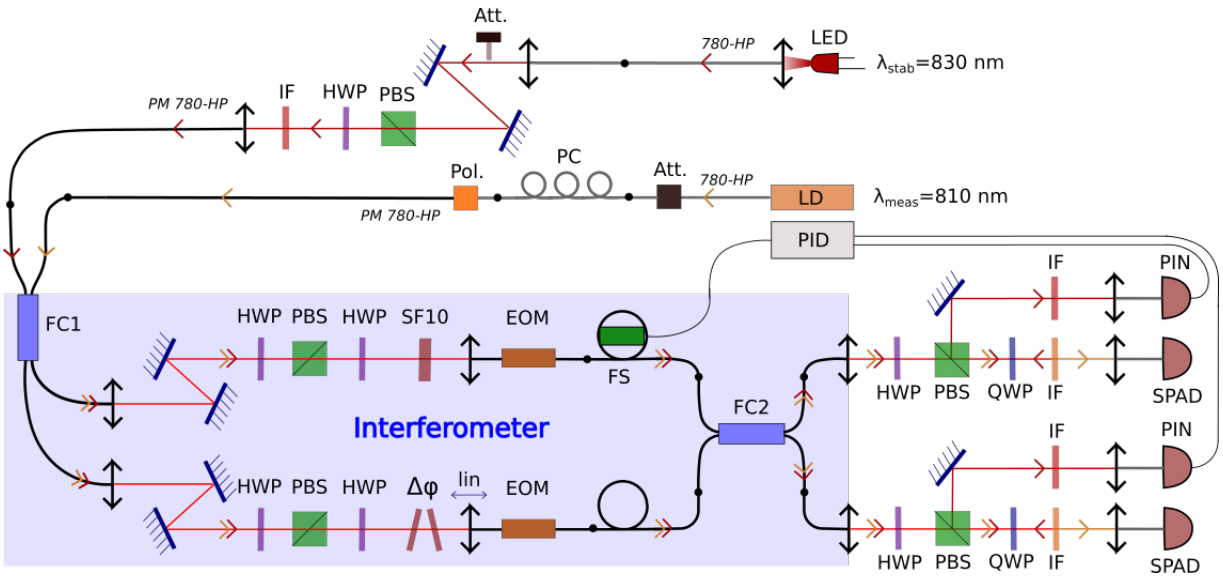

Figure 12: Mach-Zehnder interferometer operating with two optical signals. Firstly, the signals are prepared and coupled into the slow axis of polarization-maintaining fiber (PM 780-HP). Then they pass through the interferometer. On the output, they are separated by an optical isolator and detected. One of the signals is used for stabilization, and the other is used for measurement. Legend: LD – laser diode, PC – polarization controller, Att. – attenuator, Pol. – fiber polarizer, PBS – polarizing beam splitter, HWP – half-wave plate, IF – interference filter, FC – fiber coupler, $\Delta\varphi$ – phase dispersive element, SF10 – dispersion-compensating plate, EOM – integrated electro-optic phase modulator, FS – fiber stretcher, QWP – quarter-wave plate, PIN – P-I-N photodiode, SPAD – single-photon detector.

Source of the stabilization signal is a LED with central wavelength 850 nm and FWHM≈50 nm coupled into single mode fiber 780-HP. Then it passes through an air gap. Beam splitter performs projection of the non-polarized light from LED to horizontal polarization. The half-wave plate serves for proper coupling into the slow axis of polarization-maintaining optical fiber (PM 780-HP). In the air gap, there are also placed three interference filters FL830-10 from Thorlabs. They reduce spectrum of the LED to avoid crosstalk to the measurement signal. The resulting stabilization signal has central wavelength $\lambda_{\text{stab}} = 830$ nm and FWHM=10 nm. Its

total power is controlled by an attenuator. For more details about the source of the stabilization signal, see section 3.1.

Laser diode QFLD-810-10S from QPhotonics with central wavelength $\lambda_{\text{meas}} = 810$ nm is a **source of the measurement signal**. It is coupled into single mode fiber 780-HP, but coupling to slow axis of polarization-maintaining optical fiber (PM 780-HP) is required. Hence polarization controller and fiber polarizer (FOP-11-11) are used. The total power of the signal is controlled by an attenuator. Usually, it is attenuated to single-photon level or to continuously detected but weak signal. On the other hand, while not attenuated it serves for alignment purposes.

Stabilization and measure signal mix together on fiber coupler FC2. This configuration is just provisional because another signal cannot be added to the interferometer. To utilize full 2-2 switch, another coupler has to be added. However, during this experiment, it was not necessary. Now the **interferometer** will be described. Each arm of the interferometer consists of two parts: A free space part with the length of ≈ 1 m and a fiber part with the length of ≈ 8.5 m. Thus the total optical path of each arm is ≈ 14 m.

Free space part mainly serves for precise balancing path difference of the arms ΔL. It is done with a coupling lens standing on an adjustable stage with the micrometric screw (lin). Also, the losses in each arm can be tuned, thus imperfection of splitting ratio of FC1 can be compensated and high visibility of the interferometer can be achieved. In addition, the phase dispersive element ($\Delta\varphi$) from glass SF10 is placed in one arm. It is a device for setting an arbitrary relative phase difference of the signals (see section 2.4). A static element from the same glass is added to the other arm to compensate dispersion caused by $\Delta\varphi$. Combination of HWP-PBS-HWP serves for filtering out a non-polarized light and couple again into PM 780-HP.

An integrated electro-optic phase modulator (EOM) from EOspace in the **fiber part** is used for fast phase-switching. It has high intrinsic dispersion. This is solved by adding similar EOM to the other arm. Compensation of phase fluctuations is enabled with fiber stretcher (FS) which is a part of the stabilization loop. Signals from the two arms interfere on FC2.

Signals at each output are **separated** with an optical isolator, which is a sequence of PBS, QWP and IF (see section. 2.5). To filter out background light, measurement and stabilization signal are coupled into a single-mode fiber (780-HP). The measurement signal is detected with single-photon avalanche diodes (SPAD) from Excelitas. For strong signal measurements, they were replaced by continuous detectors. Stabilization signal is detected with continuous detectors (PIN). To avoid crosstalk from measure to stabilization signal interference filter FL830-10 is placed before each detector. More details about detectors and separation part are in section. 3.2.

In this setup, the random phase fluctuation is compensated with stabilization feedback loop (see section. 2.6) including photodiodes (PIN), PID regulation, and piezoelectric fiber stretcher (FS), which is placed in one arm of the interferometer. Phase fluctuations, which correspond to intensity detected, are evaluated in PID controller. PID controller simply puts corresponding voltage to FS, thus the optical path is increased or decreased and the phase of the interferometer is compensated. This PID regulation has also built-in adaptive setpoint which responds to total

intensity fluctuation. In the next sections, the parts of the stabilization loop will be described in detail.

3.1 Source of the stabilization signal

The choice of the suitable source of the stabilization signal is crucial for a good performance of the stabilization. Its intensity has to be stable enough even if the adaptive setpoint is used. Faster intensity fluctuation could overload the PID. Also, the central wavelength drift is undesirable. According to (5), relative drift between λ_{meas} and λ_{stab} causes change of the phase difference $\Delta\varphi$. Thus in spite of properly working stabilization, the phase of the measurement signal changes.

Firstly, the frequency-stabilized semiconductor laser diode QFBGLD-830-5 (SN:07.14.351) from QPhotonics with a central wavelength $\lambda_{\mathrm{stab}} = 830$ nm was used. As a result of the frequency stabilization, no drift of the central wavelength can occur. Nevertheless, there is another problem. The laser diode has very long coherence length, thus every air gap between optical surfaces behaves like a Fabry-Perot resonator with low quality. Similar effect have reflections on fiber connections and fiber components. This unwanted interference is unstable and it results to intensity fluctuations with amplitude of $\pm 5\%$ on short-time scale and over $\pm 25\%$ on a long-time scale. It occurs on all frequencies, so the adaptive setpoint cannot compensate it properly. We tried to eliminate the fluctuations by modulating the pump current of the laser diode with the modulation frequency of ~ 10 kHz. Effectively it should modulate the central wavelength, thus reduce the coherence length of the laser diode. The pump current modulation suppressed the fluctuations mainly on frequencies (> 1 Hz). Unfortunately, there was still a slight difference between fluctuations at output port 1 and output port 2. Therefore it was impossible to balance output ports (see section 2.2). Finally, we have decided to use another source of the stabilization signal.

We use LED SFH4851 with central wavelength 850 nm and FWHM$\approx$50 nm coupled into single mode fiber. Subsequently, it passes through bandpass filters FL830-10 with maximum transmittance on 830 nm and FWHM=10 nm. Extinction on 810 nm of the single filter is $\sim 10^3$. Stabilization signal contains typically $\sim 10^9$ photons/s. Due to suppressing crosstalk to measurement signal to the minimum, the sequence of three filters is utilized. The result is spectral and intensity-stable signal. However, utilization of the LED as a stabilization source has some specific properties: Firstly, due to a low efficiency of coupling LED into the single-mode fiber, the stabilization signal has low intensity. After passing the setup it has total intensity of ~ 100 pW, however, it is still enough for stabilization. Secondly, the coherence length is short due to the broad spectrum of stabilization signal, thus the stabilization has to perform close to the maximum of the autocorrelation function. The latter issue is actually beneficial – it keeps the interferometer close to zero optical path difference where the effect of relative drift between λ_{meas} and λ_{stab} is minimal.

3.2 Detection and wavelength separation

Stabilization signal has to be weak enough to have no crosstalk with the measurement signal. To detect weak signals, the detector has to be sensitive enough. On the other hand, with increasing gain of the detector its bandwidth decreases. Therefore the resulting optical power of stabilization signal is a trade-off between crosstalk and speed of the stabilization loop.

We use two types of detectors: The first one is extremely sensitive PDF 10A from Thorlabs with gain 10^{12} $\frac{\mathrm{V}}{\mathrm{W}}$ and noise-equivalent power (NEP) 1.4 $\frac{\mathrm{fW}}{\sqrt{\mathrm{Hz}}}$. It has 3 dB bandwidth of ≈ 30 Hz. For sufficient stabilization, it is necessary to have signal-to-noise ratio (SNR) more than 100. It corresponds to optical power of ~ 1 pW. The second one is picowatt photoreciever PWPR-2K-SI-FS from Femto. It has gain 10^{10} $\frac{\mathrm{V}}{\mathrm{A}}$, NEP 9 $\frac{\mathrm{fW}}{\sqrt{\mathrm{Hz}}}$ and 3 dB bandwidth of 2 kHz. When we use full bandwidth, the optical power has to be ~ 100 pW.

For wavelength separation, interference filter LL01-810-12.5 from Semrock is used in each output port. It has the maximum transmittance at ≈ 810 nm, FWHM ≈ 3 nm, and extinction at ≈ 830 is 10^8. Resulting crosstalk is only ≈ 10 photons/s from stabilization to measurement signal which is less than dark counts of used SPADs.

3.3 PID controller

The PID controller employed is an extension of the version described in [29]. Scheme of PID controller is in Fig. 13. It is fully analogue and utilizes operational amplifiers LM358N with negative feedback. Its dynamic range is from -15 V to +15 V. The controller consists of 6 independent parts: Adaptive setpoint (Aset), difference (-), proportional (P), integral (I), derivative (D), and summation (+) term.

The signals from detectors $U_{\mathrm{in1,2}}$ go to the **adaptive setpoint term**, where are balanced to the same level and summed with a gain g. Mathematically,

$$U_{\mathrm{set}} = g \cdot (U_{\mathrm{in1}} + b \cdot U_{\mathrm{in2}}), \tag{18}$$

where the b is coefficient of balance.

The sum corresponds to the intensity of stabilization beam and the gain g sets the desired phase of the interferometer (setpoint). The g is in range of 0 to 1. The balance and setpoint, parameters b and g respectively, are adjustable by potentiometers. Fast changes of setpoint would overload the feedback loop, thus it includes also low-pass filter with cut-off frequency of ≈ 1 Hz.

Note: It is also possible to use external setpoint. In this case, there is only U_{in1} and the adaptive setpoint term is omitted.

In the **difference term**, U_{in1} and U_{set} are subtracted and the result is error signal U_{err}. It is proportional to actual error of phase. Mathematically,

$$U_{\mathrm{err}} = U_{\mathrm{in1}} - U_{\mathrm{set}}. \tag{19}$$

Than U_{err} is divided to P,I, and D term.

In the **proportional term** (P), the U_{err} is just amplified with adjustable gain in range of 0 to 8.3.

In the **integral term** (I), the low frequencies of U_{err} are amplified. There are four switchable cut-off frequencies (0.3 Hz, 0.7 Hz, 6 Hz, 30 Hz). The gain is in range of 0 to 83. The integral term is important for long time stability.

In the **derivative term** (D), the high frequencies of U_{err} are amplified. Basically, it is a high-pass filter with four switchable cut-off frequencies (190 Hz, 400 Hz, 1 kHz, 3.4 kHz). The gain is in range of 0 to 8.3. The derivative term damps oscillations of the feedback loop.

Than the signals from P,I, and D term are summed in the **summation term** and amplified with gain g_s in the range of 0 to 83,

$$U_{\text{out}} = g_s(U_P + U_I + U_D). \tag{20}$$

This term also includes low-pass filter to suppress the high-frequency noise. U_{out} is applied to piezoelectric fiber stretcher to compensate phase changes.

An advanced version of PID controller is under development. Firstly, it will be based on low-noise and low-drift operational amps, thus noise of the system will be decreased. Secondly, for more variability, the number of settings and monitoring outputs will be increased. Thirdly, its dynamical range will be doubled.

3.4 Fiber stretcher

Fiber stretcher is the last part of the feedback loop. It is placed in one arm of the interferometer. It consists of a piezoelectric crystal mounted in mechanical parts and around them a long fiber is wounded [26]. A voltage applied to the piezo crystal changes its length and the fiber is stretched. Thus the fiber stretcher changes the optical path linearly with the applied voltage. Therefore output voltage from PID controller U_{out} compensates the phase fluctuations when the PID parameters are set properly. A high dynamic range of the fiber stretcher and the PID controller is important for compensating large drifts and reaching the long-time stability of the interferometer. Our aluminum fiber stretcher developed and described in [26] has the dynamic range of $\pm 330\pi$ for $\lambda = 810$ nm when the maximum range of voltage -30 V to $+150$ V is used. In reality, our dynamic range is limited by PID controller. Its dynamic range is from -15 V to $+15$ V. It corresponds to $\pm 55\pi$ for $\lambda = 810$ nm, which is usually still enough for a few hour phase-lock. Another important parameter is frequency response. It determines the possible speed of the feedback loop. Due to the high capacity of the piezo crystal (7.2 μF) it has 3 dB bandwidth of about 1 kHz.

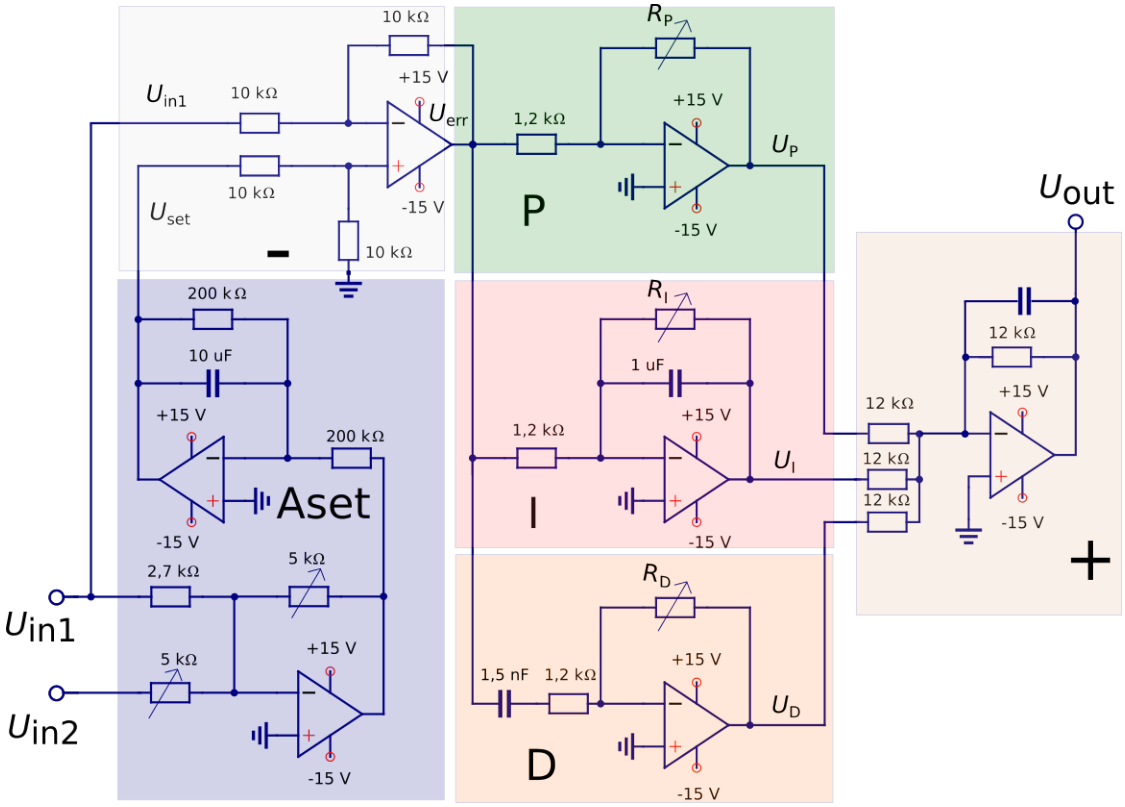

Figure 13: Scheme of PID controller. It consists of 6 parts: adaptive setpoint (Aset), difference (-), proportional (P), integral (I), derivative (D), and summation (+) term. Input signals $U_{\mathrm{in1,2}}$ are evaluated in adaptive setpoint term into U_{set}, which goes together with U_{in1} to difference term. U_{set} and U_{in1} are subtracted, the result is U_{err} which corresponds to actual phase error. U_{err} is divided into P,I, and D terms, where the signal is frequency-modified. In integral term, low frequencies are amplified. In derivative term, high frequencies are amplified. These frequency-dependent signals are then summed and amplified in summation term. The summation term also includes low-pass filter to avoid oscillations of the feedback loop. It is also possible to use external setpoint, then there is just one input (U_{in1}) and the adaptive setpoint circuit is omitted.

4 Results

Mach-Zehnder interferometer can be interpreted as a beam splitter with a variable splitting ratio as shown in Fig. 14. Incident beam is divided into output ports with splitting ratio $T : R$ depending on phase φ in the interferometer. Using the phase dispersive element we are able to tune arbitrary splitting ratio and simultaneously stabilize in the middle of the interference fringe. Moreover, while using fast electro-optic phase modulator we are able to switch the splitting ratio in the scale of nanoseconds without disruption of the stabilization process. These are major advantages of this interferometric *beam splitter*. The first part of this section is about the stability of splitting ratio using stabilization feedback loop and continuously detected (strong) measurement signal. The second part of this section is about single-photon measurements,

especially about the fast switching of splitting ratio. The splitting ratio tuning procedure is described in Appendix B.

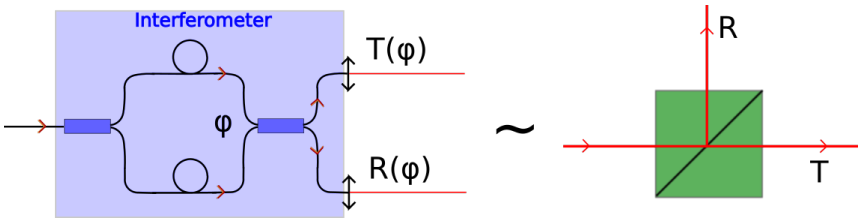

Figure 14: Interpretation of an interferometer as a beam splitter.

4.1 Charactarization using strong signal

Firstly we demonstrated stability and variability of splitting ratio using continuously detected measurement signal. We set 9 different splitting ratios from the lowest to the highest one and we kept them for 3 min. Particular measurements were assembled together and resulting *stairway* graph is shown in Fig. 15(a). Only the transmittance T is shown, however, the reflectance R can be easily evaluated from $T + R = 1$. Fig. 15(b) shows mean value and standard deviation of T. In the second column, there is information about a drift of T. The drift is a difference between T at the beginning and at the end of the measurement. The values of standard deviation and drifts vary due to the randomness of phase fluctuations in the lab. Also, settings of PID parameters were varied. In addition, there was a difference between stabilization light sources. For the newest measurements $T = 49.9$ and $T = 25.5$ was used LED, and for the others frequency-stabilized laser diode was utilized (see section 3.1).

To investigate the stability more precisely, we have done a measurement for splitting ratio 50:50 with duration of 15 min. It was chosen as 50:50 due to highest derivation of intensity $\frac{dI}{d\varphi}$. Thus the change of the phase causes the highest change of the splitting ratio. Time progress of the splitting ratio is shown in Fig. 16(a). Mean transmittance of the measurement signal is $(50.0 \pm 0.1)\%$. The drift of transmittance is only 0.037% per 15 min. Suppressing of the drift is crucial for long-time stability since the drift changes mean value of transmittance. Besides of the measurement signal, stabilization signal and voltage applied to fiber stretcher U_{out} is also shown. U_{out} reflects the phase fluctuations and slow phase drift included its direction. The phase drift of $\approx \pi$ was compensated. It would correspond to change of transmittance from 0.5 to 0 and again to 0.5 without the stabilization.

Frequency picture given as Fourier transform of the time progress is shown in Fig. 16 (b). The spectral power density of compensated phase fluctuations decreases linearly in log-log scale. It reflects the fact that integration term compensating slow drift is dominant in the stabilization process. It helped to reduce slow drift ($f < 10^{-1}$ Hz) in 6 orders. Frequencies higher than 10^{-1} Hz and less than 10 Hz were suppressed as well, but with rapidly decreasing efficiency. However, fluctuations on these frequencies are not significant. Nevertheless, for the stabilization signal, the fluctuations are suppressed at least till 50 Hz. It is consistent with 3 dB bandwidth of the

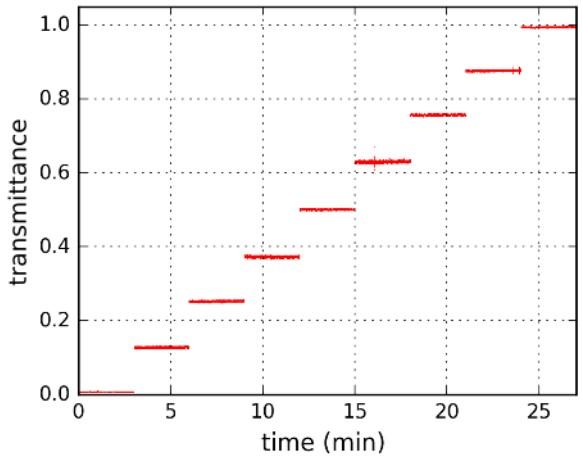

transmittance (%)	drift (%)
99,3 ± 0,1	-0,070
87,5 ± 0,1	-0,253
75,5 ± 0,2	-0,070
62,9 ± 0,2	-0,247
49,9 ± 0,1	-0,003
37,1 ± 0,2	0,099
25,1 ± 0,1	-0,196
12,6 ± 0,1	-0,084
0,59 ± 0,06	-0,043

(b)

Figure 15: Demonstration of variability of the splitting ratio $T : R$. (a) Graph of transmittance T. reflectance is just $R = 1 - T$, thus it is not shown. (b) Values of transmittance T with drift, which describes how the T was changed during the measurement.

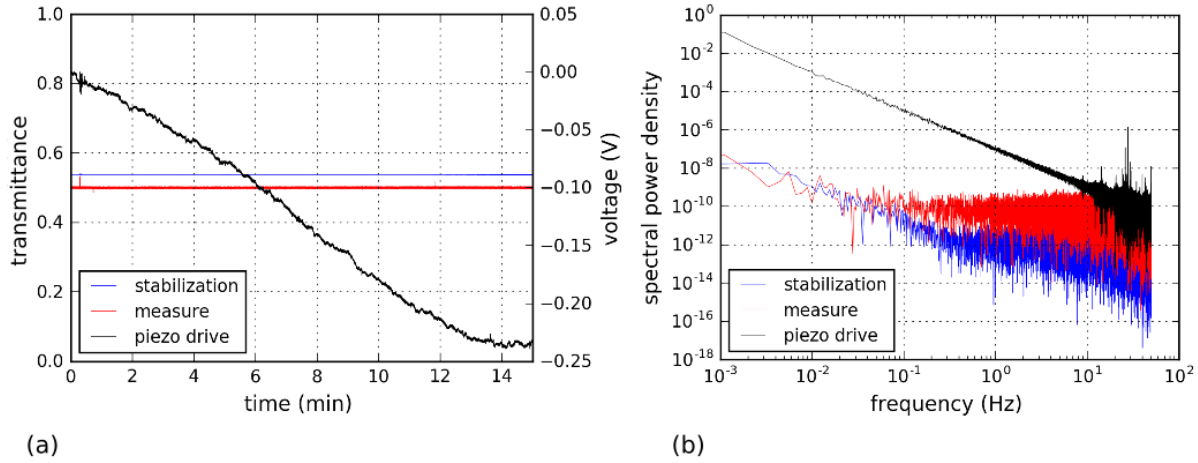

Figure 16: Demonstration of stability of the splitting ratio $T : R$. Besides the transmittance for measure signal (red) it is shown transmittance for stabilization signal (blue) and voltage applied to fiber stretcher (black). It reflects compensated phase fluctuations. (a) time progress (b) frequency picture

stabilization loop which is 30 Hz and 1 kHz, respectively, depending on used detectors. The difference between phase-lock efficiency for stabilization and measurement signal is probably a consequence of the other effects as a local change of refractive index and its dispersion or wavelength fluctuations of the measurement signal. These effects can not be eliminated easily, however, it will be the subject of the future research.

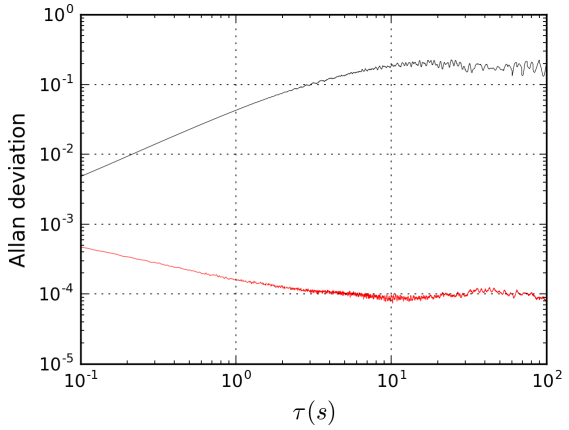

Figure 17: Allan deviation of transmittance for non-stabilized interferometer (black) comparing to active stabilized interferometer (red).

As well we evaluated Allan deviation shown in Fig. 17. It shows the error of transmittance depending on integration time τ (see section 2.7). For non-stabilized interferometer (black) the Allan deviation increases until $\tau = 10$ s and then it saturates on value 0.2. The saturation is caused by the limited range of transmittance. For stabilized interferometer (red), the Allan deviation decreases[3] until $\tau = 10$ s and then it is roughly constant with a value of $\approx 10^{-4}$. For $\tau > 10\,\mathrm{s}$ it is the improvement of precision in the order of 10^3. However, for higher τ (beyond the range shown) the Allan deviation would increase due to the slight occurrence of the slow drift.

4.2 Single-photon measurements

In the previous section, stabilization was tested on the continuously detected signal. In this section measurement signal is attenuated to single-photon level. Firstly, measurement of stabilization performance for different splitting ratios on single-photon level was done. Secondly, fast switching of phase enabled with electro-optic phase modulator was performed.

Measurement of stability for 5 different transmissivities from the lowest one to the highest one is shown in Fig. 18 (a). Exact values of the transmissivities are shown in Fig. 18 (b). We reached extinction corresponding to the maximal visibility of the setup $V_{\max} = 99.56\%$. It corresponds to the transmissivities$(0.22 \pm 0.04)\%$ and $(99.78 \pm 0.02)\%$,respectively. Drifts of the ultimate values are extremely low. For $(99.78 \pm 0.02)\%$ drift is even smaller than the measurement precision. It is a consequence of low derivation $\frac{dI_{\mathrm{out1}}}{d\varphi}$, thus random phase fluctuation causes the lowest change of transmittance. For many experiments the configuration of splitting ratio 0:100 or 100:0 is convenient. Further, switches performing in this configuration will be presented.

This single-photon measurement is slightly different from the measurement with the continuous signal. Due to the Poissonian characteristic of laser light, every measured sample has uncertainty done as a square root of the number of counts. To provide sufficient precision of the

[3] The decrease is caused by averaging of faster fluctuations

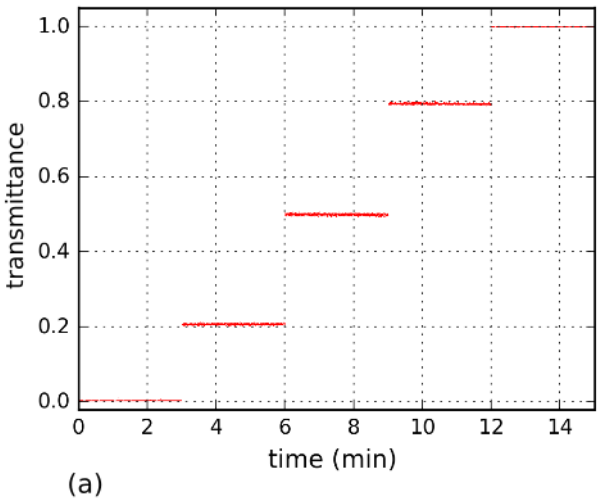

transmittance (%)	drift (%)
99,78 ± 0,02	0,00
79,3 ± 0,2	0,12
49,8 ± 0,2	0,17
20,6 ± 0,2	-0,10
0,22 ± 0,04	0,016

(b)

Figure 18: Single-photon measurement of stability for different splitting ratios $T : R$. (a) Graph of transmittance T. reflectance is just $R = 1 - T$, thus it is not shown. (b) Mean values of transmittance T with drift, which describes how the T was changed during the measurement.

measurement, each sample has a duration of 100 ms. Count rate of single-photon signal is approximately $600 \cdot 10^3$ counts/s, thus every sample with duration 100 ms contains $(60.0 \pm 0.2) \cdot 10^3$ counts. However, this value is split to output ports with splitting ratio $T : R$. Provided the total intensity is constant[4], transmittance 1%, 50%, and 99% for a single sample is measured with precision of $(1.00 \pm 0.05)\%$, $(50.0 \pm 0.3)\%$, and $(99.00 \pm 0.05)\%$ respectively. Thus measured fluctuation of transmittance consists of real fluctuation caused by phase fluctuations of the interferometer and a fluctuation of count rate caused by the Poissonian statistic of the light. Hence standard deviations and drifts from Fig. 18 (b) and Fig. 15(b) can not be easily compared.

However, there were also different conditions during the single-photon and continuous measurement. Firstly, the continuous signal was sampled with the frequency of 100 Hz with no low-pass filter, but sampling frequency of single-photon signal was only 10 Hz. Thus faster fluctuation of transmittance during single-photon accumulation process are averaged. Secondly, LED as a stabilization signal source was used in all of the single-photon measurements. Thirdly, single-photon measurement was done without setup covering, thus passive stability was worse.

The second measurement done on single-photon level is fast switching of splitting ratio. Scheme of the fast switching is in Fig. 19. The splitting ratio is changed with a fast electro-optic phase modulator (EOM). It is controlled with pulses generated in a pulser. To control the amplitude of the pulses, a radio-frequency (RF) attenuator is utilized. It has lowest tuning step 0.1 dB and the highest attenuation is 12 dB. It enables us to switch to various splitting ratios with high resolution. An optical signal is detected with single-photon avalanche detector (SPAD). When a photon is detected, SPAD generates an electronic pulse. Each pulse goes

[4]It is satisfied for short-scale measurements.

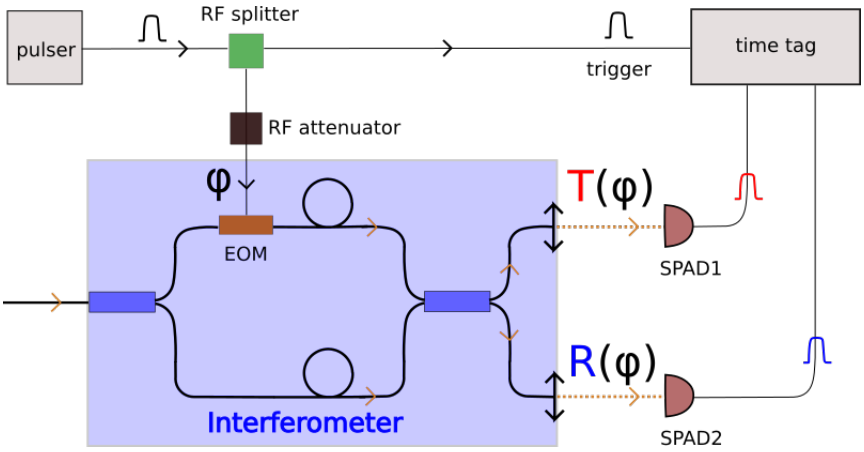

Figure 19: Scheme of fast switching of splitting ratio. EOM – integrated electro-optic phase modulator, SPAD – single-photon avalanche detector.

through a coaxial cable to an electronic device called time-tag, which assigns to each pulse a hardware bin with the resolution of 162 ps. Since it is important to have an information when the splitting ratio was switched, a part of each switching pulse is split-off by an unbalanced RF splitter and goes to the time-tag as well. The pulse serves as a trigger, thus it allows us to evaluate correctly which photons were affected by the splitting ratio switching.

Examples of the fast splitting ratio switching done with this setup are shown in Fig. 20. The switching was performed with a pulse with FWHM= 5 ns and with the repetition rate of 360 kHz. To demonstrate tunability of the switching we choose three different switching splitting ratios 50:50 (a), 20:80 (b), and 0:100 (c). When the splitting ratio is not switched, it is locked on $100 : 0$. Exact values of the splitting ratios are shown in Fig. 20 (d). The values are evaluated by equations (2) and (3). We evaluated the splitting ratios from data of duration 2.6 ns when the pulses reached their maximum.

Total count rate was 40000-60000 counts per bin, depending on the measurement. It corresponds to relative uncertainty $\pm 0.4\%$. Dark counts of used SPADs from Excelitas are in the range of 3-4 per bin for the blue channel and in range of 25-40 for the red channel. When the signal is switched to the minimum, dark counts are 3-9% of the signal. The dark counts were not subtracted from the signal.

Deformation of rising edge of the pulses in Fig. 20 (a) and (b) is caused by using one RF attenuator extra. Generally, the attenuation negatively affects the shape of pulses, thus it is sufficient to avoid the higher amount of attenuation. During this measurements it was in the range from 4.8 dB to 12 dB. Important parameter for characterization frequency response of switching is a rise time defined as 10%-90% of the amplitude of the pulse. For pulses from in Fig. 20 (c) the rise time is 0.7 ns. However, the most limiting factor should be jitter of SPADs which is ≈ 0.4 ns. Hence the pulse was probably slightly affected by the attenuators as well.

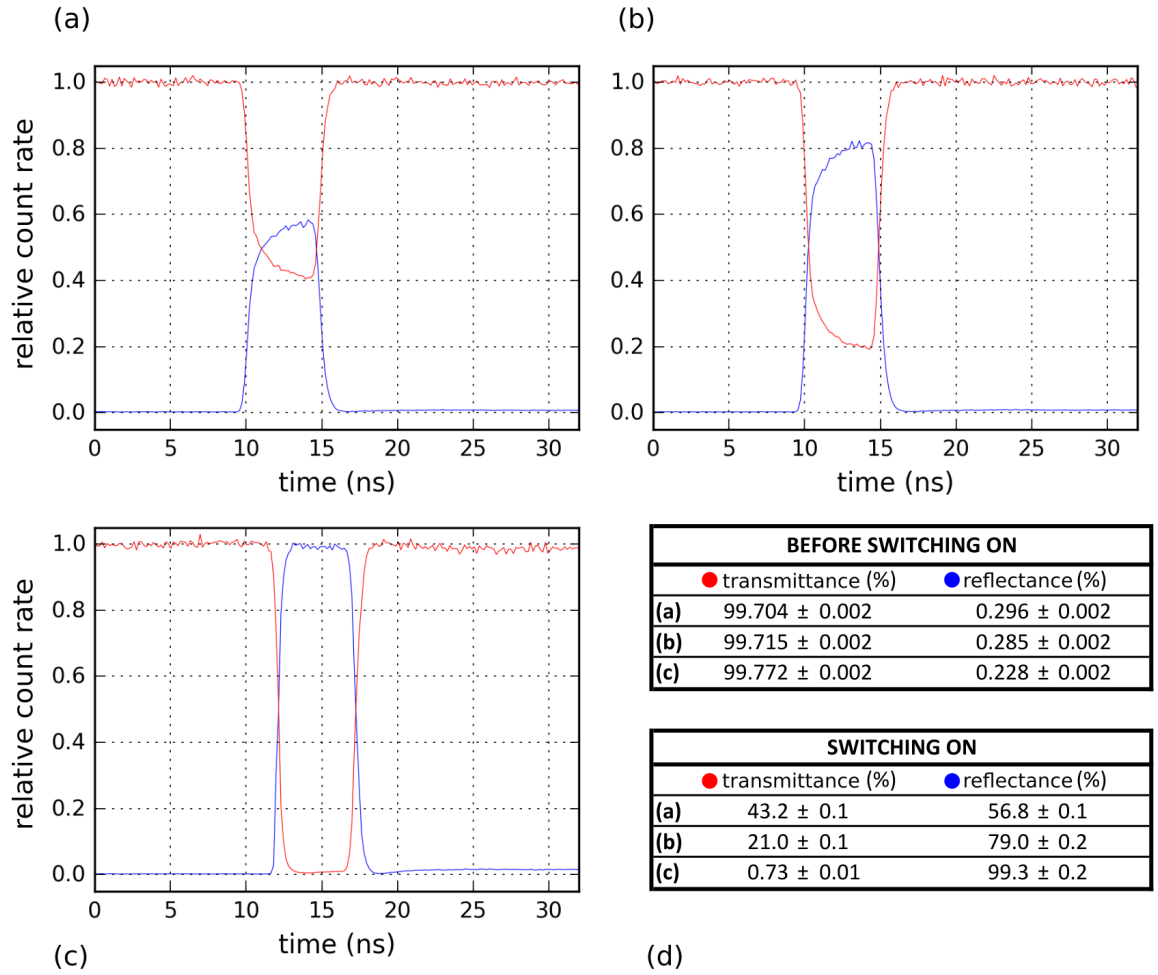

BEFORE SWITCHING ON		
	transmittance (%)	reflectance (%)
(a)	99.704 ± 0.002	0.296 ± 0.002
(b)	99.715 ± 0.002	0.285 ± 0.002
(c)	99.772 ± 0.002	0.228 ± 0.002

SWITCHING ON		
	transmittance (%)	reflectance (%)
(a)	43.2 ± 0.1	56.8 ± 0.1
(b)	21.0 ± 0.1	79.0 ± 0.2
(c)	0.73 ± 0.01	99.3 ± 0.2

Figure 20: Fast switching of various splitting ratios. The splitting ratio starts from 100 : 0 and it is switched to 50 : 50 (a), 20 : 80 (b), 0 : 100, (c). Exact values evaluated from equations (2) and (3) are shown in (d).

In Fig. 20 (c) it is well-observed that splitting ratio after the pulse does not return to previous value. It is a consequence of the switching pulse shape. The pulse has a *tail* with opposite polarity and duration of about 160 ns that is perfectly transferred by the EOM.

Now a bit discussion about maximal extinction ($\frac{T_{\max}}{R_{\min}}$ or $\frac{R_{\max}}{T_{\min}}$) feasible with this setup: When the interferometer is tuned to maximize visibility on one output port $V_1 = 99.56\%$, than on the other port is visibility $V_2 = 99.4\%$. Then extinction for switched and non-switched splitting ratio is different. Switch presented here was set to have higher visibility V_1 for the port which is denoted such as reflectance (blue). In this configuration, the extinction for the blue port is 450 (26.6 dB) and for the red port it is 332 (25.2 dB).

Although the maximal repetition rate was not our main object of interest, we experimentally tested the pulses with the repetition rate up to 5 MHz, which is the maximal repetition rate of the pulser. The switching did not affect the stabilization performance at all. The reason is that the pulse duration is much lower than the response time of the stabilization.

5 Conclusion

The main task of this Thesis is to actively stabilize fiber Mach-Zehnder interferometer for single-photon measurements. Active phase-lock is performed with an auxiliary stabilization signal, ultra-sensitive photodiodes, custom PID controller, and custom fiber stretcher. The stabilization signal is much stronger than the single-photon measurement signal, and they are differentiated by the wavelength. The stabilization runs continuously and independently of the single-photon measurements.

All the experimental challenges, such as selection of a suitable source of the stabilization signal, and separation of the stabilization and measurement signal at the outputs, were successfully solved. We also solved a task how to set an arbitrary phase difference between the stabilization and the measurement signal. We proposed and implemented custom phase dispersive element for this experiment. Also, we improved the analog PID controller from [29] implemented in the active phase-lock.

We demonstrated that the phase-locked interferometer can operate as a variable ratio coupler. The splitting ratio is controlled by the phase in the interferometer. We set 9 different splitting ratios from 0:100 to 100:0 and characterize their long-term stability. The best performance is for ultimate values 0:100 and 100:0. However, even for the most sensitive value of 50:50 the error is only 0.1% during 3 minutes. Furthermore, we investigated long-term performance of the phase-lock. Slow phase drifts up to 0.1 Hz, which are dominant, were suppressed by 6 orders of magnitude. 3 dB bandwidth of the stabilization loop is 1 kHz. Using Allan deviation, we investigated the error of transmittance (splitting ratio) in dependence of data accumulation time. For measurement time more than 10 s, there was 3 orders improvement comparing to the non-stabilized interferometer.

In the second part, we demonstrated on the single-photon level that the setup can perform fast switching of the splitting ratio. We perform the switching with integrated electro-optic phase modulator placed in one arm of the interferometer. We switched various splitting ratio for 5 ns with a rise time of 0.7 ns, and there is still some space for further improvements. Still, it is much better than the response of commercial switches. Even for one of the fastest [30], the rise time is more than 10 ns. Moreover, our implementation of optical switch can perform with repetition rate at least 5 MHz comparing to $\sim$100 kHz of the commercial devices. Our extinction of 25 dB is comparable to the extinction of the commercial switches. However, any arbitrary splitting ratio can be set

Our setup will be utilized for single-photon experiments in Quantum Optics Lab Olomouc. Using the fast switching as a part of feed-forward, interesting applications such as quantum thermodynamics simulations or modification of statistics of light are envisioned.

References

[1] L. Zehnder. Ein neuer interferenzrefraktor. *Zeitschrift für Instrumentenkunde*, 11:275–285, 1891.

[2] C. Zhao and J. H. Burge. Vibration-compensated interferometer for surface metrology. *Applied optics*, 40(34):6215–6222, 2001.

[3] M. C. Barbosa, I. de Oliveira, and J. Frejlich. Feedback operation for fringe-locked photorefractive running hologram. *Optics Communications*, 201(4):293 – 299, 2002.

[4] H. Iwai, C. Fang-Yen, G. Popescu, A. Wax, K. Badizadegan, R. R. Dasari, and M. S. Feld. Quantitative phase imaging using actively stabilized phase-shifting low-coherence interferometry. *Optics Letters*, 29(20):2399–2401, 2004.

[5] I. Marcikic, H. De Riedmatten, W. Tittel, H. Zbinden, and N. Gisin. Long-distance teleportation of qubits at telecommunication wavelengths. *Nature*, 421(6922):509, 2003.

[6] X.-s. Ma, S. Zotter, J. Kofler, R. Ursin, T. Jennewein, Č. Brukner, and A. Zeilinger. Experimental delayed-choice entanglement swapping. *Nature Physics*, 8(6):479, 2012.

[7] G. Carvacho et al. Postselection-Loophole-Free Bell Test Over an Installed Optical Fiber Network. *Physical Review Letters*, 115(3):030503, 2015.

[8] F. Vedovato, C. Agnesi, M. Tomasin, M. Avesani, J.-A. Larsson, G. Vallone, and P. Villoresi. Post-selection-loophole-free Bell violation with genuine time-bin entanglement. *arXiv:1804.10150v2*, 2018.

[9] E. Knill, R. Laflamme, and G. J. Milburn. A scheme for efficient quantum computation with linear optics. *Nature*, 409:46–52, 2001.

[10] M. Miková, H. Fikerová, I. Straka, M. Mičuda, J. Fiurášek, M. Ježek, and M. Dušek. Increasing efficiency of a linear-optical quantum gate using electronic feed-forward. *Physical Review A*, 85(1):012305, 2012.

[11] J. Claudon, J. Bleuse, N. S. Malik, M. Bazin, P. Jaffrennou, N. Gregersen, C. Sauvan, P. Lalanne, and J.-M. Gérard. A highly efficient single-photon source based on a quantum dot in a photonic nanowire. *Nature Photonics*, 4(3):174, 2010.

[12] A. L. Migdall, D. Branning, and S. Castelletto. Tailoring single-photon and multiphoton probabilities of a single-photon on-demand source. *Physical Review A*, 66(5):053805, 2002.

[13] G. J. Mendoza, R. Santagati, J. Munns, E. Hemsley, M. Piekarek, E. Martín-López, G. D. Marshall, D. Bonneau, M. G. Thompson, and J. L. O'Brien. Active temporal and spatial multiplexing of photons. *Optica*, 3(2):127–132, 2016.

[14] F. Kaneda and P. G. Kwiat. High-efficiency single-photon generation via large-scale active time multiplexing. *arXiv preprint arXiv:1803.04803*, 2018.

[15] J. G. Rarity, P. R. Tapster, and E. Jakeman. Observation of sub-Poissonian light in parametric downconversion. *Optics Communications*, 62(3):201–206, 1987.

[16] G. Brida et al. An extremely low-noise heralded single-photon source: A breakthrough for quantum technologies. *Applied Physics Letters*, 101(22):221112, 2012.

[17] S. Takeda and A. Furusawa. Universal Quantum computing with Measurement-Induced Continuous-Variable Gate Sequence in a Loop-Based Architecture. *Physical Review Letters*, 119:120504, 2017.

[18] D. Pulford, C. Robillard, and E. Huntington. Single photon locking of an all-fiber interferometer. *Review of Scientific Instruments*, 76(6):063114, 2005.

[19] S.-B. Cho and T.-G. Noh. Stabilization of a long-armed fiber-optic single-photon interferometer. *Opt. Express*, 17(21):19027–19032, 2009.

[20] G. B. Xavier and J. P. von der Weid. Stable single-photon interference in a 1 km fiber-optic Mach–Zehnder interferometer with continuous phase adjustment. *Opt. Lett.*, 36(10):1764–1766, 2011.

[21] M. Miková. *Quantum optical experiments focused on quantum information processing*. Ph.D. Thesis, Department of Optics, Faculty of Science, Palacký University Olomouc, 2017.

[22] M. Hendrych, M. Dušek, and O. Haderka. The effect of beam-splitter imperfections and losses on fringe visibility in a Mach-Zehnder interferometer. *Acta Physica Slovaka*, 46:393–398, 1996.

[23] B. E. A. Saleh and M. C. Teich. *Fundamentals of Photonics*. Wiley interscience - 2. edition, New Jersey, 2007.

[24] Refractive index database. [online], 2. 5. 2018. https://refractiveindex.info.

[25] K. J. Astrom and T. Hagglund. *PID controllers*. International Society for Measurement and Control, 2nd ed. Research Triangle Park, 1995.

[26] L. Podhora. *Charakterizace a konstrukce vláknového fázového modulátoru*. Bachelor's thesis, Department of Optics, Faculty of Science, Palacký University Olomouc, 2015.

[27] D. W. Allan. Statistics of atomic frequency standards. *Proceedings of the IEEE*, 54(2):221–230, 1966.

[28] D. V. Land, A. P. Levick, and J. W. Hand. The use of the Allan deviation for the measurement of the noise and drift performance of microwave radiometers. *Measurement Science and Technology*, 18(7):1917, 2007.

[29] V. Švarc. *Aktivní fázová stabilizace interferometru pomocí zpětnovazební PID regulace.* Bachelor's thesis, Department of Optics, Faculty of Science, Palacký University Olomouc, 2016.

[30] NanoSpeed 1x2 Solid-State Variable Fiberoptic Splitter from Agiltron. https://agiltron.com/product/ns-high-speed-optical-variable-splitter/.

Appendix

A Data processing

During the strong signal measurements utilizing photodiodes (sec. 4.1), the data were sampled with 16-bit analogue-digital converter (ADC) with sampling frequency 100 Hz.

Our algorithm written in Python serves for evaluating phase φ (splitting ratio $T : R$). It enables real-time tuning of φ and post-processing of φ. Real-time tuning was used especially for tuning specific $T : R$ in section 4.1 and for better precision averaging over 100 samples was done. The algorithm operates with both outputs of the interferometer, thus it takes into account total intensity changes caused by intensity fluctuations of the laser diode and setup detuning. It proceeds similarly to procedure described in section 2.2, see eq. (6) – eq. (8). For the phase evaluation the eq. (8) is used. There are two main parts of the algorithm:

In the first part, a file called *beforecheck* is imported. It is the check of parameters just before the measurement and it consists of two parts: The first is just information about offsets of electronic devices (especially detectors) and the second is a scan of interference fringes in both outputs OUT1 and OUT2. This serves for subtracting offsets off1 and off2 and for evaluating visibilities V_1 and V_2 according to equations (1) and (6). Then signal from OUT2 is balanced to correspond to eq. (8). The quality of balancing is checked graphically, where total intensities I_{out1} and I_{out2} are displayed (by the program). Values of visibilities V_1 and V_2 are written to *.txt* file called *VIS*.

The second part serves for evaluation of φ from the main measurement. Firstly, data from measurement are imported. Secondly, each sample is evaluated in *for* cycle using eq. (8). If some error occurs during data sampling and a sample cannot be interpreted as a *float*, the cycle simply omits it. The results of φ are exported to *.csv* file.

B Splitting-ratio tuning procedure

Firstly, we tried to set specific splitting ratio deterministically. It means that we expected that for a specific angle of rotation α of the dispersive element we achieve specific splitting ratio. The precision of this method was horrible, roughly $\pm 30\%$. The main reason is that the exact place in autocorrelation function is hardly achievable due to its flatness. Also, change of phase is too fast and random thus it is impossible to set specific splitting ratio deterministically. Thus, in reality, this process is mostly heuristic and iterative.

Firstly it is necessary to adjust the setup to reach the highest visibility of the measurement signal. This is crucial especially if splitting ratio 100:0 or 0:100 are set. Then the PID controller is adjusted which means that proper PID parameters are set and balancing of U_{in1} and U_{in2} is done. It provides the correct performance of the adaptive setpoint. The setpoint is set approximately to 90°. Then short measurement called *beforecheck* is done. Its purpose is to measure offset of electronic devices and to find out visibilities of the measure and stabilization signal. The

beforecheck is used in a script which evaluates exact splitting ratio. Then exact splitting ratio is sought. It is an iterative process: We switch on the stabilization and look which splitting ratio is set. If it is close to the desired one, we just fine-tune it with stabilization setpoint. If not, we switch off the stabilization and tune it again with the phase dispersive element. This is done iteratively. If phase change caused by the phase dispersive element is too high, it is necessary to balance optical path of the interferometer again. Also, it is necessary to do the *beforecheck* again due to possible visibility change.

C Photo of the experiment

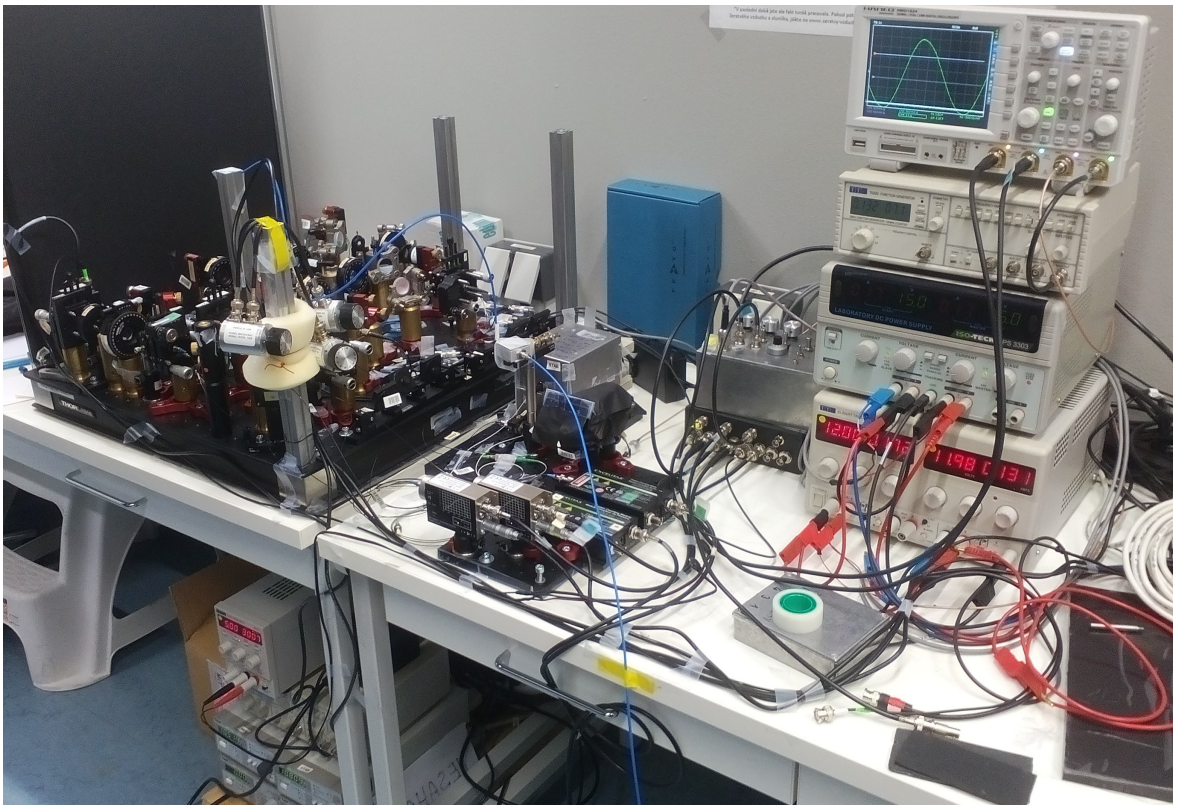

Figure 21: Photo of the experimental setup. On the left side, there is the fiber Mach-Zehnder interferometer without covering. In the middle part, there are detectors, PID controller, and laser diodes. On the right side, there are power supplies, function generator, oscilloscope, and ADC. Under the table, there is power supplier of SPADs, controllers of laser diodes. Computer for data sampling and counting electronics are not shown in the figure.